Synthesis, Characterization, and Antioxidant Activity of a New Copper(II)-imidazole Derivative Complex

Ariel Colaço de Oliveira [a], Ana Claudia Pedrozo da Silva [a], Antonio Gustavo Sampaio de Oliveira-Filho [b], Lilian Tatiani Dusman Tonin [a], André Luiz Tessaro [a], Felipe N. Pererira [b], Jonas de Arruda Leite Junior [b], and Rafael Block Samulewski* [a]

Degenerative diseases such as cancer, cataract, and cerebral dysfunction are increasingly associated with free radicals. Copper(II) complexes exhibit antioxidant activity and can act in the treatment of these diseases altering or inhibiting cellular functions by intercalations with nitrogenous bases of DNA. Those complexes can be employed in the development of new drugs and materials for the treatment of these diseases or as preventive agents. In this work, we present the synthesis and characterization of a complex formed by an imidazole-type ligand and copper(II). NMR data confirm the structure of ligand and that its interaction with copper(II) ions produces the complex $[Cu(3NIMDZ-H)(OH_2)_5](ClO_4)_2$ with a coordinated binding between copper(II) ion and nitrogen of the imidazole ring. Density functional theory (DFT) calculations performed at the B3LYP-D3(BJ)/def2-SVP level of theory for both the complex and ligand reveal that the formation of the complex is spontaneous, exhibiting a copper-nitrogen bond length of 1.988 Å. The antioxidant assays showed a high-speed inhibition of complex radicals regarding free ligand. IC_{50} value is 1.5 times higher than the BHT standard, demonstrating the high antioxidant power of this compound. $[Cu(3NIMDZ-H)(OH_2)_5]^{2+}$ shows a fast kinetics behavior for DPPH inhibition, which shows the possibility of new material application in antitumoral drug development.

Graphical abstract
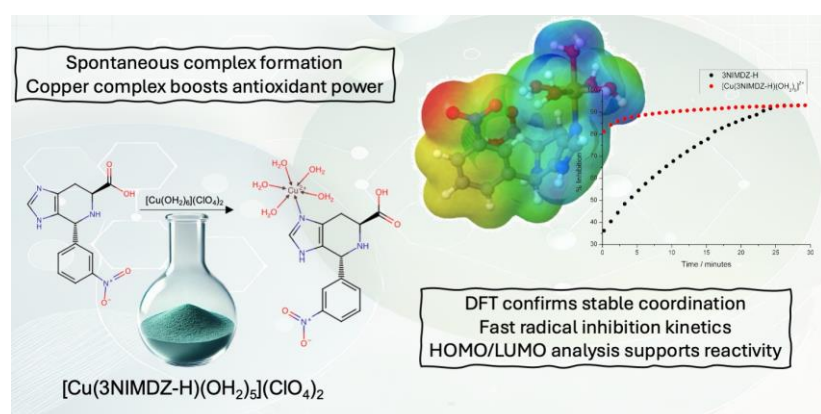
1. Introduction

Free radicals are reactive compounds that tend to capture electrons from stable biological molecules. Overproduction of free radicals happens when a pathologic condition due to the presence of pro-oxidants compounds and other risk factors,

[a] Chemistry Department, Federal Technological University of Paraná, zip code 86812-460 Apucarana, Paraná, Brazil. [b] São Carlos Institute of Chemistry, University of São Paulo, 13566-590, São Carlos, São Paulo, Brazil. *Corresponding author. E-mail: **samulewski@utfpr.edu.br**

such as smoking and stress, give rise to oxidative stress [1]. Degenerative diseases - such as cancer, cataract, cardiovascular diseases, immune system weakness, and cerebral dysfunction - are increasingly related to excess free radicals and insufficient quantity of antioxidants [2]. These antioxidants are molecules capable of delaying or inhibiting cell damage through their free radical scavenging property.

The therapeutic potential of transition metal complexes in cancer treatments has attracted much scientific interest [3-7]. Among metals, copper is an essential ion present in biological processes as many enzymes cofactor and plays a key role in transport, activation, and metabolism [8-11]. This metal has been frequently selected for the synthesis of antitumor drugs due to its lower systemic toxicity when compared to platinum [12, 13]. Copper(II) complexes can act on DNA through cavitation interactions, external electrostatic interactions, covalent interactions, and intercalations with nitrogenous bases of DNA, inhibiting cellular function [14-21].

Imidazole structure is a five-membered heterocyclic with an aromatic amine [22]. This group is present in several biological molecules, such as adenine, guanine, histidine, and natural products [23, 24]. The imidazole group stands out in chemistry, biology, and medicine due to its miscellaneous applications, such as complexes with antitumor activities [25-31]. The versatility of the imidazole group is mainly due to its structure containing two nitrogen atoms. Deprotonated nitrogen has a great potential for coordination with metal ions, and when protonated, it becomes a good donor of hydrogen bonds, interesting for supramolecular chemistry.

In this research, we developed a copper-imidazole complex, where the ligand 6-carboxy-4-(3-nitrophenyl)-imidazo-[4,5-c]-4,5,6,7-tetrahydropyridine (3NIMDZ-H) was synthesized from L-histidine. In addition to structural characterization and spectroscopic studies, Density Functional Theory (DFT) calculations were performed to investigate the charge distribution of the complex. Finally, the antioxidant activity of the complex was also evaluated through the inhibition of 2,2-diphenyl-1-picrylhydrazyl (DPPH).

2. Material and Methods

2.1 Materials

L-histidine, sodium carbonate, and 3-nitrobenzaldehyde were purchased from Synth, and butyl-hidroxytoluene (BHT), Copper(II) perchlorate $[Cu(OH_2)_6](ClO_4)_2$, and 2,2-diphenyl-1-picrylhydrazyl (DPPH) were purchased from Sigma-Aldrich. The water used was double-distilled. All solvents employed were of analytical grade and were used without further purification.

2.2 Synthesis of compound 6-carboxy-4-(3-nitrophenyl)-imidazo-[4,5-c]-4,5,6,7-tetrahydropyridine (3NIMDZ-H)

The ligand 3NIMDZ-H was synthesized by adding 6.0 equivalents of sodium carbonate (36.0 mmol, 3.82 g) and 1.0 equivalent of 3-nitrobenzaldehyde (6.0 mmol, 0.91 g) to 150 mL of a L-histidine ethanolic solution (0.04 mol L^{-1}). The reaction was kept under a reflux for 7 hours, and its evolution was accompanied by thin layer chromatography (TLC) using CHCl3/MeOH as eluent and developed with iodine vapors. After cooled, the mixture was filtered and washed with ethanol. The filtrate was collected, and the solvent was removed using a rotary evaporator. The yield was 97 %. [32]

2.3 Synthesis of complex [Cu(3NIMDZ-H)(OH$_2$)$_5$](ClO4)$_2$

$[Cu(OH_2)_6](ClO_4)_2$ solution (0.116 g, 0.3 mmol in 10 mL of ethanol) was slowly dropped on ligand 3NIMDZ-H solution (0.08 g, 0.3 mmol in 20 mL of ethanol). The result solution was kept under stirring for 10 min. Blue-green powder was isolated, washed with ethanol, ether, and air dried.

2.4 Physical Measurements

NMR ^{1}H and ^{13}C measurements were performed by Varian nuclear spectrometer model Mercury Plus BB 300 MHz at 20 °C on (DMSO-d$_6$). UV-Vis spectra in the range 190-900 nm were obtained on a Cary-60 spectrophotometer in water:DMF (1:1 v/v). Infrared spectra were obtained with a Cary-630 FTIR spectrophotometer (400-4000 cm^{-1}) in KBr pellets. Conductivity was measured in a conductometer BEL W3B comparing the complex with different 1 M inorganic salts solutions.

2.5 Computational Details

Geometry optimization, frequency, and thermochemical calculations for all structures were performed using the B3LYP density functional [33-36]. The D3 version of Grimme's dispersion with Becke−Johnson damping (D3BJ) [37] was used, with the def2-SVP basis set [38] within Orca 6.0 [39]. This level of theory, herein referred to as B3LYP-D3BJ/def2-SVP, has been shown to have satisfactory performance in predicting transition metal complexes, harmonic vibrational frequencies, and bond energies when compared to highly correlated electronic structure methods [40]. The UV-Vis absorption spectrum of the $[Cu(3NIMDZ-H)(OH_2)_5]^{2+}$ was calculated using time dependent DFT (TDDFT) with the B3LYP density functional and the def2-TZVP basis set, at the B3LYP-D3(BJ)/def2-SVP optimized geometry for the ground electronic state. All structures studied in this work were optimized in an aqueous solution using the polarizable continuum model (PCM) [41]. The nature of all stationary points was confirmed as minima by the harmonic vibrational frequency calculations with no imaginary frequencies.

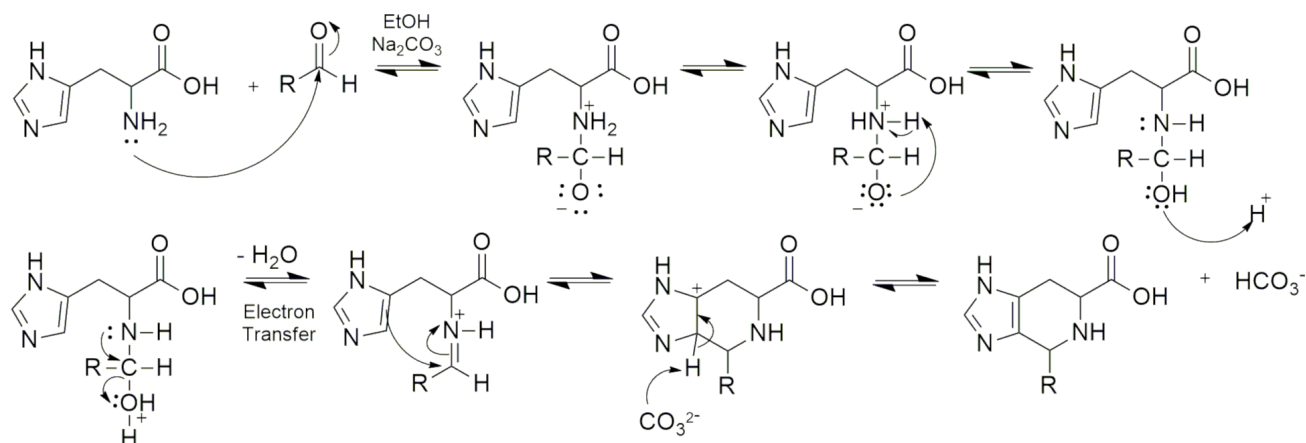## 2.6 Determination of DPPH Scavenging Activity

Several techniques have been used to determine in vitro antioxidant activity of substances to allow a rapid selection of potentially interesting compounds in the prevention of chronic degenerative diseases. Among these methods, the free radical scavenging method through DPPH is known to have purple staining absorbing at a maximum wavelength of 517 nm. At this method, by the action of an antioxidant or a radical species, the purplish DPPH is reduced by yellowish diphenyl-picryl-hydrazine formation, which can be monitored by absorbance decrease.

The DPPH scavenging method was used to measure the antioxidant activity of the 3NIMDZ-H ligand and the copper(II) complex [42, 43]. A methanolic solution of DPPH (60 µmol L^{-1}) was used for IC$_{50}$ measurements (IC$_{50}$ is the concentration at which 50% of the initial DPPH reacted). Methanolic solutions of ligand and complex were prepared with concentrations of 31.3, 62.5, 125, 50, and 100 mg mL^{-1}. For comparison, a BHT solution (600 mg mL^{-1}) was used as a standard.

In a cuvette, 2.0 mL of DPPH solution and 1.0 mL of ligand or complex solution at different concentrations were mixed. Control was prepared by adding 1.0 mL of methanol to 2.0 mL of DPPH solution. Spectrophotometric data were collected at 517 nm for 30 minutes. Antioxidant activity was expressed as the percentage of inhibition (% AA), according to Equation 1,

where Ac represents absorbance of control, Ab is the absorbance of blank sample, and Aa the absorbance of the compound solutions.

$$\%AA = \frac{Ac - (Aa - Ab)}{Ac}$$

(1)

3. Results and Discussion

3.1 NMR description of ligand

L-histidine was condensed with 3-nitrobenzaldehyde by Pictet-Spengler reaction. The proposer mechanism was described in Scheme 1. A mixture of *cis* (4S, 6S) and *trans* (4R, 6S) diastereoisomers of 3NIMDZ-H was observed and confirmed by ^{1}H and ^{13}C NMR data. (^{1}H NMR and ^{13}C NMR spectra can be visualized as Supplementary Material)

Scheme 1. Mechanistic proposal for the synthesis of imidazo-[4,5-c]4,5,6,7-tetraidropiridyne unity by Pictet-Spengler reaction.

The imidazo-[4,5-c]4,5,6,7-tetrahydropyridine unity of ligand was confirmed by H-4 shifts (δ_H 5.06 for *cis* and e δ_H 5.14 for *trans*) at ^{1}H NMR and C-4 shifts (δ_C 59.0 for *cis* and δ_C 58.3 for *trans*) at ^{13}C NMR. Furthermore, phenyl group presence at the C-H position can be observed. All data of ^{1}H and ^{13}C signals were visualized in Table 1. The numbered

structure of the synthesized ligand can be visualized in Figure 1. Three distinct large signals with shifts greater than 8.5 ppm are observed in the ^{1}H spectrum and are related to two hydrogens of the amine group and one of the carboxylic group.

Table 1. NMR signals of ^{1}H and ^{13}C for *cis* (4S, 6S) and *trans* (4R, 6S) 3NIMDZ-H diastereoisomers in DMSO-d_6. Atom numbers are according to Figure 1.

H	*cis* δ_H (multiplicity, J=Hz)	*trans* δ_H (multiplicity, J=Hz)	C	*cis* δ_C (assignment)	*trans* δ_C (assignment)
2	7.32 (*s*)	7.47 (*s*)	2	134.0 (CH)	134.3 (CH)
4	5.06 (*s*)	5.14 (*s*)	3	147.1 (C)	147.6 (C)
6	3.26 (*dd*, 3.0; 9.0)	3,11 (*dd*, 3,0; 9.0)	4	59.0 (CH)	58.3 (CH)
7α	2.72-2.83 (*m*)	2,72-2.83 (*m*)	6	53.7 (CH)	54.3 (CH)
7β	2.55-2.64 (*m*)	2.55-2,64 (*m*)	7	27.3 (CH$_2$)	27.3 (CH$_2$)
2'	8.17 (*d*, 3.0)	8.17 (*d*, 3,0)	1'	134.9 (C)	134.9 (C)
4'	8.09-8.12 (*m*)	8.09-8.12 (*m*)	2'	122.5 (CH)	121.8 (CH)
5'	7.60 (*t*, 7.0)	7,59 (*t*, 7.0)	3'	148.0 (C)	148.0 (C)
6'	7.84 (*d*, 6.0)	7,84 (*d*, 6.0)	4'	123.2 (CH)	122.3 (CH)
			5'	129.7 (CH)	129.7 (CH)
			6'	135.9 (CH)	135.9 (CH)

3.2 Complex characterization

The conductivity measurements of the complex solution (67.3 µS cm^{-1}) are comparable to the CaCl$_2$ solution 1.0 mol L^{-1} (63.8 µS cm^{-1}) and the NaCl solution 1.0 mol L^{-1} (5.8 µS cm^{-1}), indicating a cation:anion ratio of 1:2 and suggesting coordination through the nitrogen of the imine ring. Interaction of copper(II) ion by carboxylic group changes total complex charge by deprotonated ligand form (COO$^-$) and cation:anion ratio 1:1 would be observed. The conductivity measurements can give a clue about complex structures. It is expected that complex formation happens through coordination between copper(II) ion and the imine nitrogen of the imidazole ring in 3NIMDZ-H ligand. The other

coordination positions are occupied by water molecules and perchlorate, which function as a counter ion to charge neutrality to product the complex [Cu(3NIMDZ-H)(OH$_2$)$_5$](ClO$_4$)$_2$. This proposal is corroborated by Gibbs free energy ($\Delta G°$) for the [Cu(OH$_2$)$_6$]$^{2+}$ + 3NIMDZ-H → [Cu(3NIMDZ-H)(OH$_2$)$_5$]$^{2+}$ + H$_2$O reaction ($\Delta G°$ = -12.9 kcal mol^{-1}) and by the geometry optimization. This Gibbs free energy indicates the spontaneity of the exchange between a water molecule and the 3NIMDZ-H ligand in the first coordination sphere of the copper(II) ion. In addition, the optimized geometry for the [Cu(3NIMDZ-H)(OH$_2$)$_5$]$^{2+}$ complex is displayed in Figure 2a, featuring a copper-nitrogen bond length of 1.988 Å. Figure 2b illustrates the electrostatic potential map of the complex, revealing a

pronounced positive charge distribution in the vicinity of the copper(II) cation, while negative potential regions are observed near the electronegative groups of the ligand. Figure 2c depicts the lowest unoccupied molecular orbital (LUMO) of the transition metal complex which is predominantly centered on the nitrophenyl group of the

ligand. The highest occupied molecular orbital (HOMO), Figure 2d, is a singly occupied orbital predominantly centered on the copper atom, exhibiting characteristic d orbital features. The orbital energy associated with the LUMO orbital is -3.133 eV and the energy of the HOMO orbital is -6.725 eV.
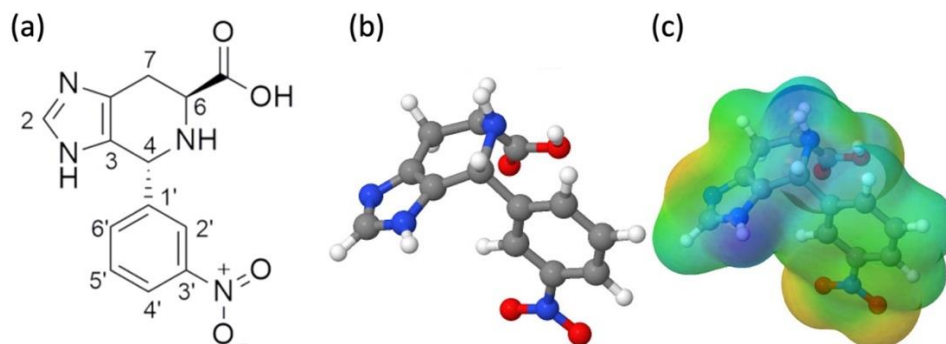

Fig. 1. (a) Structure of 3NIMDZ-H. The atom numbering follows Table 1. Hydrogen atoms have the same number as the carbon atom to which they are bonded. (b) B3LYP-D3(BJ)/def2-SVP optimized geometry for 3NIMDZ-H. (c) Electrostatic potential map generated for 3NIMDZ-H at the B3LYP-D3(BJ)/def2-SVP level of theory. The red region corresponds to a negative electrostatic potential, whereas the blue color corresponds to the positive potential.
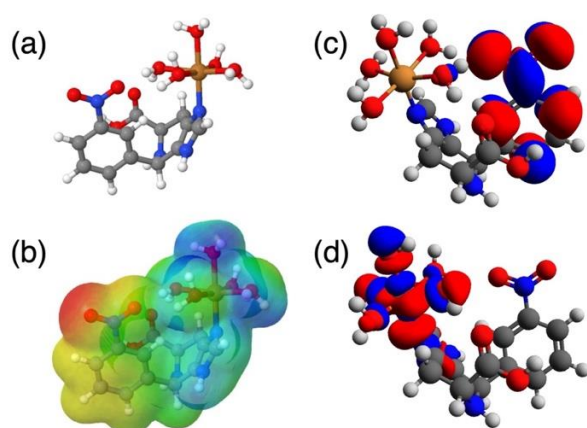

Fig. 2. (a) B3LYP-D3(BJ)/def2-SVP optimized geometry for $[Cu(3NIMDZ-H)(OH_2)_5]^{2+}$. (b) Electrostatic potential map generated for $[Cu(3NIMDZ-H)(OH_2)_5]^{2+}$ at the B3LYP-D3(BJ)/def2-SVP level of theory. The red region corresponds to a negative electrostatic potential, whereas the blue color corresponds to the positive potential. (c) Lowest unoccupied molecular orbital and (d) Singly occupied molecular orbital for $[Cu(3NIMDZ-H)(OH_2)_5]^{2+}$ at the B3LYP-D3(BJ)/def2-SVP level of theory.

The spectroscopic characterization of the samples was conducted through UV-Vis and FTIR analyses, which are illustrated in Figure 3. UV-Vis spectra (Figure 3b) show a large band at 700 nm after complexation (ε = 82,58 L mol^{-1} cm^{-1}). This band is assigned as a sum of three electronic d-d transitions (e_g-b_{1g}, b_{2g}-b_{1g} and a_{1g}-b_{1g}), typical of the tetragonal distortion of the d^9 copper(II) electronic system. The calculated natural transition orbitals [44,45] confirm this assignment and show that the three electronic transitions, involving electronic excited states S2, S3, and S4, with energies between 1.6 and 1.8 eV, are best described as pure (0.999 weight) transitions between particle/hole pairs

centered on the metal, more specifically involving the d orbitals. The pairs of NTOs for each of these transitions clearly represent d-d transitions and are displayed in Fig. 4: (a) the S0 → S2 transition, at 773 nm; (b) the S0 → S3 transition, at 769 nm; and (c) the S0 → S4 transition, at 676 nm. The calculated electronic spectrum with TDDFT, at the B3LYP-D3(BJ)/def2-TZVP level of theory, for $[Cu(3NIMDZ-H)(OH_2)_5]^{2+}$ is available in the Supporting Information as Figure 6S. FTIR characterization of ligand and complex is not trivial because the main bands were overlapping (Figure 3a). The calculated vibrational spectra, at the B3LYP-D3(BJ) level of theory, for 3NIMDZ-H and $[Cu(3NIMDZ-H)(OH_2)_5]^{2+}$ is available in the Supporting Information, as Fig. 5S.The 3NIMDZ-H ligand shows a large band at 1580 cm^{-1}, which was attributed to three bands overlapping: υ(C=O), υ(C=N), and υ(C=C), consistent with the computed vibrational spectrum at the B3LYP-D3(BJ)/def-SVP level of theory that displays such band at 1627 cm^{-1}. The bands at 1520 and 1351 cm^{-1} are correspondent to symmetric and asymmetric stretch (υ_sN-O and υ_{as}N-O) of the nitro group and corroborate with NMR obtained data. In the B3LYP-D3(BJ)/def2-SVP vibrational spectra, the υ_{as}N-O is at 1386 cm^{-1}. Finally, the band at 1406 cm^{-1} corresponds to another overlapping of C-N and C-O stretch [46, 47]. When ligand and complex spectra were compared, is perceived a large new band at 1100 cm^{-1} assigned to a typical Cl-O stretch of perchlorate as a counter ion. The major changes occur at 1406 and 1622 cm^{-1} after copper(II) coordination. This indicates that ligand coordination with copper(II) ion occurs by nitrogen of the imino ring, corroborating the conductimetric analysis. However, this analysis is not trivial, since the C=O and C-O bands of the carboxyl group occur in the same region and this group is a possible coordination site. Literature data report that histidine complexation occurs by imidazole ring as well as proposed complex $[Cu(3NIMDZ-H)(OH_2)_5](ClO_4)_2$ [47].

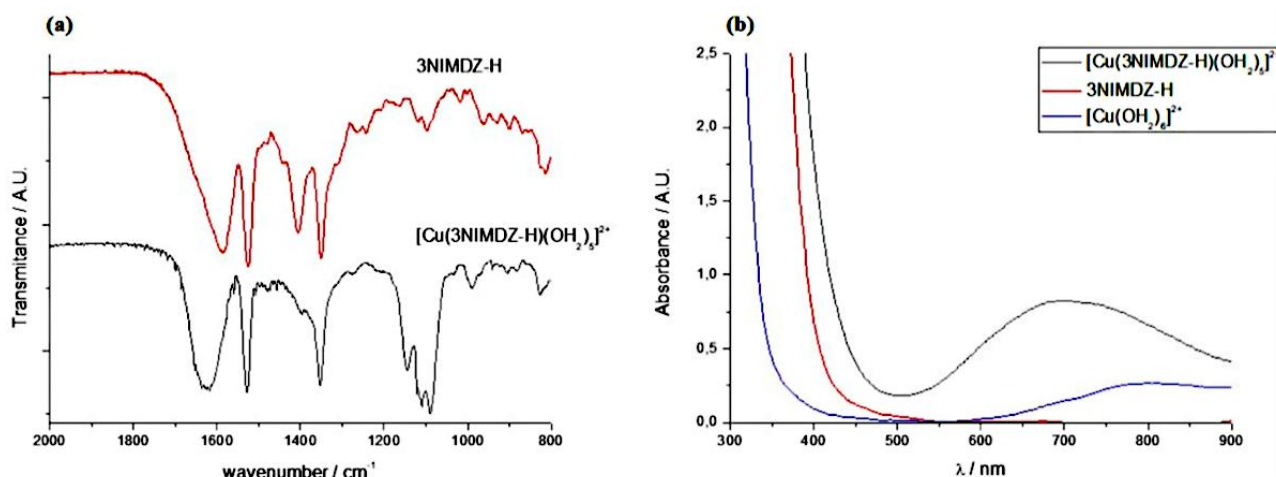**Fig. 3.** (a) FTIR spectra of 3NIMDZ-H (-) and complex [Cu(3NIMDZ-H)(OH$_2$)$_5$](ClO$_4$)$_2$ (-); (b) UV-Vis spectra of [Cu(OH$_2$)$_6$]$^{2+}$ (-), 3NIMDZ-H (-) and [Cu(3NIMDZ-H)(OH$_2$)$_5$]$^{2+}$ (-).
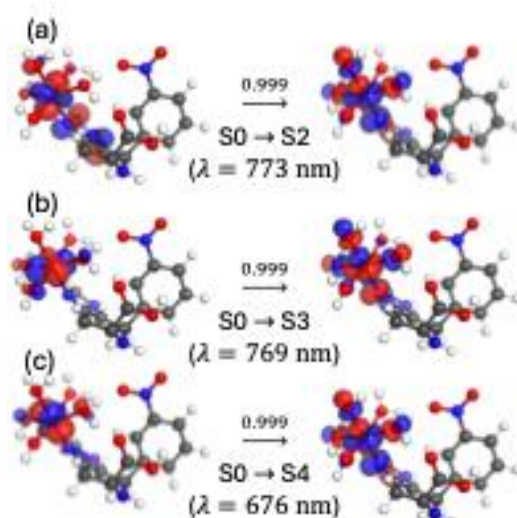

Fig. 4. Pairs of natural transition orbitals for the electronic transitions of the [Cu(3NIMDZ-H)(OH$_2$)$_5$]$^{2+}$ complex around 700 nm.

3.4 DPPH Scavenging Activity

Antioxidant activities of 3NIMDZ-H and its complex [Cu(3NIMDZ-H)(OH$_2$)$_5$]$^{2+}$ were measured by free radical DPPH inhibition. The BHT synthetic standard was chosen for its wide use in the food industry. IC$_{50}$ values obtained were 122.54 µg mL^{-1} (0.56 mmol L^{-1}) for BHT, 430.98 µg mL^{-1} (1.51 mmol L^{-1}) for ligand, and 379.22 µg mL^{-1} (0.88 mmol L^{-1}) for copper(II) complex. These values indicate a higher antioxidant activity for complex compared to ligand, suggesting that Cu^{2+} ion presence significantly changes chemical properties of the ligand. Bukhari and coworkers also observed this for quercetin [48]. Kohen and coauthors show that imidazole derivate ligands have an antioxidant activity due to hydrogen donation by the imidazole ring [49]. Esmaeili and coworkers show that copper(II) complex [Cu(His)$_2$Cl$_2$] (His = histidine) presented higher scavenging activity than free ligand histidine, representing that imidazole group function as an efficient electron donor group [50]. Thus, complexation with metal ions decreases the oxidation potential of the ligand, and the complex becomes more readily oxidized by DPPH due to greater availability of electron-donating by the imidazole ring. It is noted that IC$_{50}$ of the complex is 1.5 times higher than the BHT standard, demonstrating the significant antioxidant power of this compound.

The percentage of DPPH scavenging at times zero, 5, and 30 minutes for ligand and complex at 1000 mg mL^{-1} are shown in Table 3. Figure 5 presents the kinetic behavior of ligand and complex solutions. The kinetic behavior of the compounds can be classified according to the time of 50% DPPH radical consumption (TC$_{50}$) radical. When TC$_{50}$ is less than 5 minutes, the kinetics is classified as fast. TC$_{50}$ values between 5 and 30 minutes correspond to intermediate and slow classes [51]. These results show that the complex has faster kinetics than the ligand, inhibiting 81.31 ± 1.37% of the radical at zero time (t = 0). After 30 minutes of reaction, stabilization was notorious, and percentage values of DPPH inhibition higher than 91% for the two compounds was observed. According to this classification, the complex [Cu(3NIMDZ-H)(OH$_2$)$_5$]$^{2+}$ shows a fast kinetics, and the ligand intermediate kinetics.

Table 3. Percentage of DPPH scavenging activity at different times for ligand and complex at 1000 µg mL^{-1} and the BHT standard at 600 µg mL^{-1}

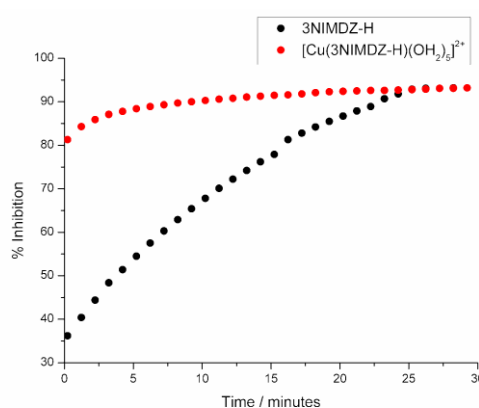| Time (min)	BHT	(3NIMDZ-H)	[Cu(3NIMDZ-H)(OH$_2$)$_5$]$^{2+}$
0.0	45.27 ± 0.25	36.19 ± 1.97	81.31 ± 1.37
5.0	70.48 ± 0.44	54.47 ± 2.15	88.41 ± 1.14
30.0	92.38 ± 0.24	91.58 ± 0.54	93.28 ± 1.11

Fig. 5. Kinetic behavior of DPPH inhibition for (●) 3NIMDZ-H ligand and (●) complex [Cu(3NIMDZ-H)(OH$_2$)$_5$](ClO$_4$)$_2$. [Sample] = 1.0 mg mL^{-1}.

4. Conclusions

Copper(II) interaction with 3NIMDZ-H (imidazole type ligand) produces the complex [Cu(3NIMDZ-H)(OH$_2$)$_5$](ClO$_4$)$_2$ and shows a coordinated binding between copper(II) ion and nitrogen of imidazole ring. NMR data confirmed the structure of the 3NIMDZ-H ligand, and FTIR analysis and computational calculation also confirmed the binding. Antioxidant assays showed a high rate of inhibition of the complex concerning the free ligand. In addition, IC$_{50}$ values highlighted the antioxidant power of the complex. Finally, the results demonstrate that both the ligand and the complex are potential precursors for the development of materials for biomedical applications.

Acknowledgments

Author Contributions

Ariel Colaço de Oliveira: conceptualization, methodology, formal analysis, validation, investigation, data curation and writing - original draft. Ana Claudia Pedrozo da Silva: conceptualization, methodology, formal analysis, writing - original draft. Antonio G. S. de Oliveira-Filho: conceptualization, methodology, formal analysis, resources, writing - original draft, supervision, project administration and funding acquisition. Lilian Tatiani Dusman Tonin: conceptualization, resources, writing - original draft, supervision, project administration and funding acquisition. André Luiz Tessaro: conceptualization, resources, writing - original draft, supervision, project administration and funding acquisition. Rafael Block Samulewski: conceptualization, resources, writing - original draft, supervision, project administration and funding acquisition.

References and Notes

[1] Ferreira, I.; Barros, L.; Abreu, R. *Curr. Med. Chem.* **2009**, *16*, 1543. **[Crossref]**

[2] Silva, D. C.; Cerchiaro, G.; Honório, K. M. *Quim. Nova* **2011**, *34*, 300. **[Crossref]**

[3] Halliwell, B. *Lancet* **2000**, *355*, 1179. **[Crossref]**

[4] Zhang, P.; Sadler, P. J. *J. Organomet. Chem.* **2017**, *839*, 5. **[Crossref]**

[5] Ponte, F.; Ritacco, I.; Mazzone, G.; Russo, N.; Sicilia, E. *Inorganica Chim. Acta* **2018**, *470*, 325. **[Crossref]**

[6] Zhao, J.; Wang, D.; Xu, G.; Gou, S. *J. Inorg. Biochem.* **2017**, *175*, 20. **[Crossref]**

[7] Song, X. D.; Kong, X.; He, S. -F.; Chen, J. -X.; Sun, J.; Chen, B. -B.; Zhao, V.; Mao, Z.-W. *Eur. J. Med. Chem.* **2017**, *138*, 246. **[Crossref]**

[8] Barin, R.; Rashid-Nadimi, S.; Biria, D.; Asadollahi, M. A. *Electrochim. Acta* **2017**, *247*, 1095. **[Crossref]**

[9] Wang, C.; Liang, X.; Tao, C.; Yao, X.; Wang, Y.; Wang, Y.;

[10] Li, K. *Biochem. Biophys. Res. Commun.* **2017**, *488*, 496. **[Crossref]**

[10] Dawkes, H. *Curr. Opin. Struct. Biol.* **2001**, *11*, 666. **[Crossref]**

[11] Zoroddu, M. A. et al. *J. Inorg. Biochem.* **2019**, *195*, 120. **[Crossref]**

[12] Trudu, F.; Amato, F.; Vaňhara, P.; Pivetta, T.; Peña-Méndez, E. M.; Havel, J. *J. Appl. Biomed.* **2015**, *13*, 79. **[Crossref]**

[13] Doucette, K. A.; Hassell, K. N.; Crans, D. C. *J. Inorg. Biochem.* **2016**, *165,* 56. **[Crossref]**

[14] Urquiza, N. M.; Islas, M. S.; Ariza, S. T.; Jori, N.; Martínez Medina, J. J.; Lavecchia, M. J.; López Tévez, L. L.; Lezama, L.; Rojo, T.; Williams, P. A. M.; Ferrer, E. G. *Chem. Biol. Interact.* **2015**, *229*, 64. **[Crossref]**

[15] Chew, S. T.; Lo, K. M.; Lee, S. K.; Heng, M. P.; Teoh, W. Y.; Sim, K. S.; Tan, K. W. *Eur. J. Med. Chem.* **2014**, *76*, 397. **[Crossref]**

[16] Ma, T.; Xu, J.; Wang, Y.; Yu, H.; Yang, Y.; Liu, Y.; Ding, W.; Zhu, W.; Chen, R.; Ge, Z.; Tan, Y.; Jia, L.; Zhu, T. *J. Inorg. Biochem.* **2015**, *144*, 38. **[Crossref]**

[17] Jia, L.; Shi, J.; Sun, Z.; Li, F.; Wang, Y.; Wu, W.; Wang, Q. *Inorganica Chim. Acta* **2012**, *391*, 121. **[Crossref]**

[18] Jia, L.; Cai, H.; Xu, J.; Zhou, H.; Wu, W.; Li, F.; Wang, Y.; Pei, X.; Wang, Q. *Inorg. Chem. Commun.* **2013**, *35*, 16. **[Crossref]**

[19] Zhu, T.; Chen, R.; Yu, H.; Feng, Y.; Chen, J.; Lu, Q.; Xie, J.; Ding, W.; Ma, T. *Mol. Med. Rep.* **2014**, *10*, 2477. **[Crossref]**

[20] Xu, J.; Zhou, T.; Xu, Z. -Q.; Gu, X. -N.; Wu, W. -N.; Chen, H.; Wang, Y.; Jia, L.; Zhu, T. -F.; Chen, R. -H. *J. Mol. Struct.* **2017**, *1128*, 448. **[Crossref]**

[21] Jopp, M.; Becker, J.; Becker, S.; Miska, A.; Gandin, V.; Marzano, C.; Schindler, S. *Eur. J. Med. Chem.* **2017**, *132*, 274. **[Crossref]**

[22] Balaban, A. T.; Oniciu, D. C.; Katritzky, A. R. *Chem. Rev.* **2004**, *104*, 2777. **[Crossref]**

[23] Dolensky, B.; Nam, G.; Deng, W. -P.; Narayanan, J.; Fan, J.; Kirk, K. L. *J. Fluor. Chem.* **2004**, *125*, 501. **[Crossref]**

[24] Rasapalli, S.; Kumbam, V.; Dhawane, A. N.; Golen, J. A.; Lovely, C. J.; Rheingold, A. L. *Org. Biomol. Chem.* **2013**, *11*, 4133. **[Crossref]**

[25] Scarpellini, M.; Neves, A.; Hörner, R.; Bortoluzzi, A. J.; Szpoganics, B.; Zucco, C.; Nome Silva, R. A.; Drago, V.; Mangrich, A. S.; Ortiz, W. A.; Passos, W. A. C.; de Oliveira, M. C. B.; Terenzi, H. *Inorg. Chem.* **2003**, *42*, 8353. **[Crossref]**

[26] Kaps, L.; Biersack, B.; Müller-Bunz, H.; Mahal, K.; Münzner, J.; Tacke, M.; Mueller, T.; Schobert, R. *J. Inorg. Biochem.* **2012**, *106*, 52. **[Crossref]**

[27] Mahal, K.; Biersack, B.; Schruefer, S.; Resch, M.; Ficner, R.; Schobert, R.; Mueller, T. *Eur. J. Med. Chem.* **2016**, *118*, 9. **[Crossref]**

[28] Espósito, B. P.; Najjar, R. *Coord. Chem. Rev.* **2002**, *232*, 137. **[Crossref]**

[29] Süleymanoğlu, N.; Ustabaş, R.; Alpaslan, Y. B.; Ünver, Y.; Turan, M.; Sancak, K. *J. Mol. Struct.* **2011**, *989*, 101. **[Crossref]**

[30] El kihel, A.; Essassi, E. M.; Bauchat, P. *Arab. J. Chem.* **2012**, *5*, 523. **[Crossref]**

[31] Beauchard, A.; Jaunet, A.; Murillo, L.; Baldeyrou, B.;

Lansiaux, A.; Chérouvrier, J. -R.; Domon, L.; Picot, L.; Bailly, C.; Besson, T. *Eur. J. Med. Chem*. **2009**, *44*, 3858. **[Crossref]**

[32] Karuso, P.; Shengule, S. Synthesis of ageladine A and analogs thereof for treatment of hyperproliferative disorders or angiogenic diseases. PCT Int. Appl. (2009) US Patent Number 2009152584.

[33] Becke, A. D. *J. Chem. Phys.* **1992**, *96*, 2155. **[Crossref]**

[34] Lee, C.; Yang, W.; Parr, R. G. *Phys. Rev. B* **1988**, *37,* 785. **[Crossref]**

[35] Vosko, H.; Wilk, L.; Nusair, M. *Can. J. Phys*. **1980**, *58*, 1200. **[Crossref]**

[36] Stephens, P. J.; Devlin, F. J.; Chabalowski, C. F.; Frisch, M. J. *J. Phys. Chem.* **1994**, *98,* 11623. **[Crossref]**

[37] Grimme, S.; Ehrlich, S.; Goerigk, L. *J. Comput. Chem*. **2011**, *32*, 1456. **[Crossref]**

[38] Weigend, F.; Ahlrichs, R. *Phys. Chem. Chem. Phys*. **2005**, *7,* 3297. **[Crossref]**

[39] Neese, F. *Wiley Interdiscip. Rev. Comput. Mol. Sci*. **2022**, *12*, e1606. **[Crossref]**

[40] Aoto, Y. A.; DiStasio Jr., R. A.; Head-Gordon, M. *J. Chem. Theory Comput.* **2017**, 13, 5291. **[Crossref]**

[41] Garcia-Ratés, M.; Neese, F. *J. Comput. Chem*. **2020**, *41*, 922. **[Crossref]**

[42] Miliauskas, G.; Venskutonis, P. R.; van Beek, T. A. *Food Chem*. **2004**, *85,* 231. **[Crossref]**

[43] Brand-Williams, W.; Cuvelier, M. E.; Berset, C. *LWT - Food Sci. Technol*. **1995**, *28*, 25. **[Crossref]**

[44] Plasser, F.; Wormit, M.; Dreuw, A. *J. Chem. Phys*. **2014**, *141*, 024106. **[Crossref]**

[45] Plasser, F.; Bäppler, S. A.; Wormit, M.; Dreuw, A. *J. Chem. Phys*. **2014**, *141*, 024107. **[Crossref]**

[46] Madhavan, J.; Aruna, S.; Thomas, P. C.; Vimalan, M.; Rajasekar, S. A.; Sagayaraj, P. *Cryst. Res. Technol.* **2007**, 42, 59. **[Crossref]**

[47] Noguchi, T.; Inoue, Y.; Tang, X. S. *Biochemistry* **1999**, *38*, 10187. **[Crossref]**

[48] Bukhari, S. B.; Memon, S.; Mahroof-Tahir, M.; Bhanger, M. I. *Spectrochim. Acta Part A Mol. Biomol. Spectrosc*. **2009**, *71*, 1901. **[Crossref]**

[49] Kohen, R.; Yamamoto, Y.; Cundy, K. C.; Ames, B. N. *Proc. Natl. Acad. Sci.* **1988**, *85,* 3175. **[Crossref]**

[50] Esmaeili, L.; Perez, M. G.; Jafari, M.; Paquin, J.; Ispas-Szabo, P.; Pop, V.; Andruh, M.; Byers, J.; Mateescu, M. A. *J. Inorg. Biochem.* **2019***, 192*, 87. **[Crossref]**

[51] Sánchez-Moreno, C.; Larrauri, J. A.; Saura-Calixto, F. *J. Sci. Food Agric.* **1998**, *76*, 270. **[Crossref]**

How to cite this article